Available online at www.sciencedirect.com
SCIENCE DIRECT®
Polyhedron 22 (2003) 3529–3539
POLYHEDRON
www.elsevier.com/locate/poly

Lanthanide complexes of 2-hydroxynicotinic acid: synthesis, luminescence properties and the crystal structures of $[Ln(HnicO)_2(\mu\text{-}HnicO)(H_2O)] \cdot nH_2O$ (Ln = Tb, Eu)

Paula C.R. Soares-Santos [a], Helena I.S. Nogueira [a,*], João Rocha [a], Vitor Félix [a], Michael G.B. Drew [c], Rute A. Sá Ferreira [b], Luís D. Carlos [b], Tito Trindade [a]

[a] Department of Chemistry, University of Aveiro, CICECO, 3810-193 Aveiro, Portugal
[b] Department of Physics, University of Aveiro, CICECO, 3810-193 Aveiro, Portugal
[c] Department of Chemistry, University of Reading, Whiteknights, Reading RG6 6AD, UK

Received 18 July 2003; accepted 30 September 2003

Abstract

New lanthanide complexes of 2-hydroxynicotinic acid (H_2nicO) $[Ln(HnicO)_2(\mu\text{-}HnicO)(H_2O)] \cdot nH_2O$ (Ln = Eu, Gd, Tb, Er, Tm) were prepared. The crystal structures of the $[Tb(HnicO)_2(\mu\text{-}HnicO)(H_2O)] \cdot 1.75H_2O$ (**1**) and $[Eu(HnicO)_2(\mu\text{-}HnicO)(H_2O)] \cdot 1.25H_2O$ (**2**) complexes were determined by X-ray diffraction. The 2-hydroxynicotinate ligand coordinates through *O*,*O*-chelation to the lanthanide(III) ions as shown by X-ray diffraction and the infrared, Raman and NMR spectroscopy results. Photoluminescence measurements were performed for the Eu(III) and Tb(III) complexes. Lifetimes of 0.592 ± 0.007 and 0.113 ± 0.002 ms were determined for the Eu^{3+} and Tb^{3+} emitting states, $^5D_0$ and $^5D_4$, respectively. A value around 30% was found for the $^5D_0$ quantum efficiency. The energy transfer mechanisms between the lanthanide ions and the ligands are discussed and compared with those observed in similar complexes involving the 3-hydroxypicolinate ligand based on the luminescence of the respective Gd^{3+}-based complexes.

Keywords: Lanthanide complexes; 2-Hydroxynicotinic acid; Luminescence; Crystal structures

1. Introduction

In the last few years, there has been intense research on the synthesis of photoactive lanthanide complexes [1–3]. Although trivalent lanthanide ions have weak absorption coefficients, in some cases highly luminescent lanthanide complexes have been prepared by chelating strongly absorbing organic ligands to the lanthanide ions [4,5]. In such cases a synergistic effect occurs between the ligand and the lanthanide ion. This is often referred as the antenna-effect: the absorbed energy by the ligand, which has a broad intense absorption band, is transferred intra-molecularly to the lanthanide ion, emitting part of this energy within a narrow-wavelength region [3]. The possibility of having ligands that function as light-harvesting units in lanthanide complexes has been investigated [4,5]. We have been particularly interested in the study of the photoluminescence behaviour of these type of lanthanide complexes associated to the study of the coordination modes of aromatic N and O donor ligands, such as 3-hydroxypicolinic acid [6], picolinic acid [7] and 2,6-dihydroxybenzoic acid [8]. Other lanthanide complexes with aromatic ligands containing nitrogen and oxygen donors have been reported, such as with nicotinate [9,10], picolinate [11], dipicolinates [12], 2,2′-bipyridine-6,6′-dicarboxylate [13] and bis-pyridones [14].

The 2-hydroxynicotinic acid (H_2nicO) ligand used in the present work is a potential chelating ligand with different chelating modes [15] including *N*,*O*-chelation

* Corresponding author. Tel.: +351234370727; fax: +351234370084.
E-mail address: helena@dq.ua.pt (H.I.S. Nogueira).

0277-5387/$ - see front matter © 2003 Published by Elsevier Ltd.
doi:10.1016/j.poly.2003.09.018

(of the monodeprotonated ligand, $HnicO^-$, through the pyridine nitrogen and the deprotonated phenolate oxygen, forming a four-membered chelate ring) or *O,O*-chelation (through the carboxylate group and the deprotonated phenolate oxygen, forming a six-membered chelate ring, salicylato type chelation [16,17], either of the twice deprotonated ligand, $nicO^{2-}$, or, as found in this work, of the monodeprotonated $HnicO^-$ ligand with a protonated pyridinic nitrogen). The ketonic tautomer of H_2nicO is stabilized by resonance and exists predominantly in a zwitterionic form (Scheme 1) in solutions at pH range 3–10.5 [18].

Few complexes of H_2nicO have been isolated, in an earlier study on second- and third-row transition metal complexes we reported the synthesis and characterization of solid Pd(II), Pt(II), Re(V), Mo(VI) and W(VI) complexes [15]. The crystal structures of the compounds *trans*-$[PdCl(HnicO)(PPh_3)_2]\cdot 0.75CH_3CN$ and *cis*-$[PtCl(HnicO)(PPh_3)_2]\cdot 0.75CH_3OH\cdot 0.5H_2O$ show the $HnicO^-$ ligand coordinated to palladium or platinum through the nitrogen atom only [15]. Solution studies were reported for gallium(III) complexes [19], in which the 2-hydroxynicotinate ligand is bound by the deprotonated phenolate and carboxylate oxygens, the pyridine nitrogen being protonated. Other solution studies include complexes of V(IV) [20], Al(III) [21,22], Cu(II) [23,24] and Hg(II) [25].

Here the synthesis of the lanthanide(III) complexes $[Ln(HnicO)_2(\mu\text{-}HnicO)(H_2O)]\cdot nH_2O$ (Ln = Eu, Gd, Tb, Er, Tm) is reported together with their characterization using vibrational and NMR spectroscopy. The chelation modes of the ligand to the different lanthanides are discussed on the basis of the X-ray crystal structures of $[Tb(HnicO)_2(\mu\text{-}HnicO)(H_2O)]\cdot 1.75H_2O$ (**1**) and $[Eu(HnicO)_2(\mu\text{-}HnicO)(H_2O)]\cdot 1.25H_2O$ (**2**), and spectroscopic results, and compared to our previous published data for analogous compounds [6]. The crystal structures of the Tb(III) and Eu(III) complexes, prove conclusively that the 2-hydroxynicotinate functions as a salicylato type ligand with *O,O*-chelation in the solid metal complexes. Spectroscopic data are consistent with the Gd(III), Er(III) and Tm(III) complexes having the same type of coordination. The local environment of the lanthanide ions in these compounds is further discussed on the basis of their luminescence properties.

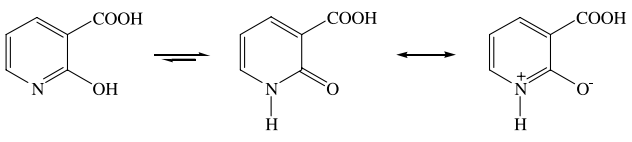

Scheme 1.

2. Results and discussion

2.1. Preparation of lanthanide(III) 2-hydroxynicotinate complexes

Aqueous solutions of Ln(III) (Ln = Eu, Gd, Tb, Er, Tm) ions and H_2nicO were stirred over one hour to give a series of lanthanide complexes with the 2-hydroxynicotinate ligand. The lanthanide complexes were characterized based on the crystal structures, spectroscopic data and elemental analysis. The crystal structures of **1** and **2** and the elemental analysis results are in accordance with the molecular formula $[Ln(HnicO)_2(\mu\text{-}HnicO)(H_2O)]\cdot nH_2O$ for all the complexes (Ln = Eu, Gd, Tb, Er, Tm). The gadolinium complex of 3-hydroxypicolinic acid (HpicOH), $[Gd(picOH)_2(\mu\text{-}HpicO)(H_2O)]\cdot 5H_2O$, was synthesized by stirring an aqueous suspension of $Gd(OH)_3$ and HpicOH, using our earlier reported method [6] for other lanthanide complexes. The spectroscopic results of the latter compound matched those obtained for the previously reported lanthanide 3-hydroxypicolinate complexes [6]. The Gd(III) complex of HpicOH was prepared in order to compare energy transfer mechanisms between the lanthanide ions and the $HnicO^-$ and $HpicO^-$ ligands, based on the luminescence of the respective Gd^{3+}-based complexes.

2.2. Crystal structures

The X-ray single crystal diffractions show that complexes **1** and **2** are isomorphous. In the crystal structure of each complex $HnicO^-$ bridges $[Ln(HnicO)_3(H_2O)]$ (Ln = Tb(III) **1** or Eu(III) **2**) structural units into a 1D chain. Furthermore the asymmetric unit consists of one $[Ln(HnicO)_3(H_2O)]$ structural moiety and water solvent molecules with different crystallographic occupancy factors, three in **1** (1.0, 0.25 and 0.50) and two in **2** (1.0 and 0.25), which were assigned in agreement with electronic density map in order to give reasonable temperature factors for the oxygen atoms of the water molecules. An ORTEP diagram [26] of the structure of the building of the 1D polymeric chain together with labelling scheme is presented in Fig. 1(a) for **1** while the Fig. 1(b) presents the overall geometry of one chain with the terbium(III) centres drawn in the polyhedra style [27]. The structure of the Eu complex is equivalent and is not shown. Selected bond lengths and angles in the metal coordination sphere, listed in Table 1 for both complexes, show that the Eu–O distances are slightly longer than the Tb–O corresponding ones reflecting the different stereoelectronic sizes of these two metals. Each lanthanide centre is surrounded by eight oxygen atoms in a distorted coordination environment of the type triangulated dodecahedron (bisphenoid) [28]. Three $HnicO^-$ ligands are coordinated via one oxygen atom of

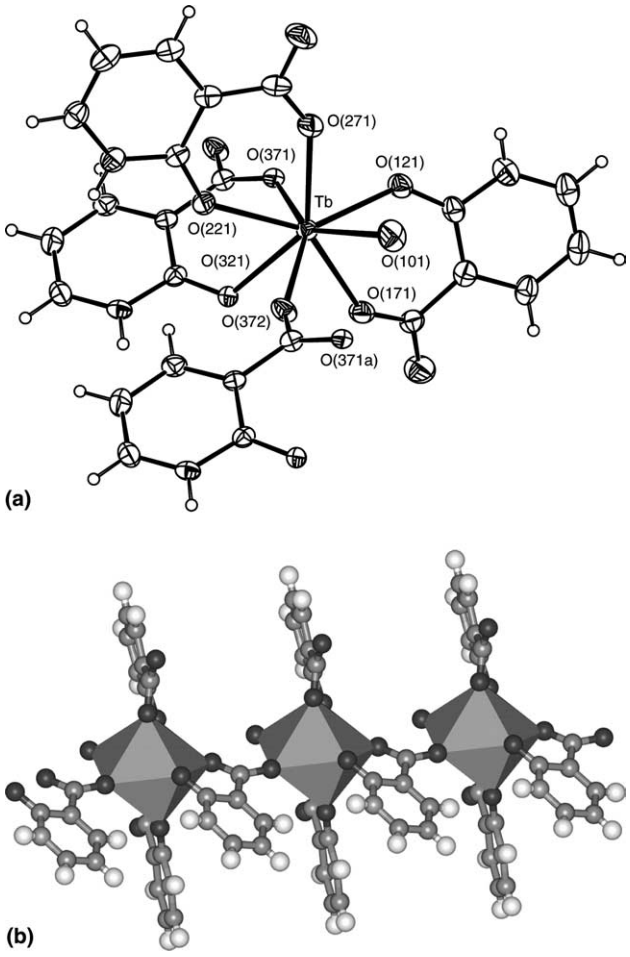

Fig. 1. Crystal structure of $[Tb(HnicO)_2(\mu\text{-}HnicO)(H_2O)]\cdot 1.75H_2O$ (**1**). (a) An ORTEP view of the building unit of **1** showing the atomic connectivities, labelling scheme adopted and the thermal ellipsoids drawn at 30% of probability level. The labels of the carbon atoms are omitted for clarity. (b) View of the polymeric $[Tb(HnicO)_2(\mu\text{-}HnicO)(H_2O)]_n$ 1D chain with the Tb^{3+} centres drawn in the polyhedra style.

Table 1
Selected bond distances (Å) and angles (°) in the lanthanide coordination spheres

	M = Tb(III) (**1**)	M = Eu(III) (**2**)
Bond distances		
M–O(121)	2.328(8)	2.353(7)
M–O(271)	2.343(8)	2.381(7)
M–O(372[a])	2.358(8)	2.388(6)
M–O(321)	2.415(6)	2.441(5)
M–O(171)	2.326(8)	2.353(7)
M–O(221)	2.362(8)	2.397(6)
M–O(371)	2.385(9)	2.439(6)
M–O(101[a])	2.480(9)	2.514(8)
Bond angles		
C(32)–O(321)–M	123.6(5)	122.5(5)
C(37)–O(372)–M[b]	155.5(7)	155.5(5)
C(37)–O(371)–M	134.7(6)	135.9(5)

Symmetry operations used to generate equivalent: [a] $x-1, y, z$; [b] $x+1, y, z$.

the carboxylate group and the oxygen atom from the phenolate group in a *O*,*O*-chelating fashion with M–$O_{carboxylate}$ distances ranging from 2.328(8)–2.385(9) Å (Tb) and 2.381(7)–2.439(6) (Eu); M–$O_{phenolate}$ distances ranging from 2.328(8)–2.415(6) Å (Tb) and 2.353(7)–2.397(6) Å (Eu), respectively. One water molecule (M–OH_2 2.480(9) Å for Tb(III) and 2.514(8) Å for Eu(III)) and one oxygen atom of a carboxylate group from a second *O*,*O*-chelated $HnicO^-$ ligand belonging to a neighbour structural unit (M–O is 2.358(8) Å and 2.388(6) Å in **1** and **2**, respectively) complete the metal coordination sphere of each complex. In the Cambridge Structural Data Base [29] there are 24 and 76 structures with TbO_8 and EuO_8 coordination polyhedra, respectively. The M–O distances are in wider ranges of distances of 2.15–2.57 and 2.15–2.80 Å for terbium and europium centres, respectively. The carboxylate group of the bridging $HnicO^-$ ligand is rotated relatively to the aromatic ring by 25.8(3)° (Tb) and 26.9(5)° (Eu) as consequence of the steric constrain imposed by the *O*,*O*-chelating mode adopted. By contrast the remaining two $HnicO^-$ ligands make angles of only 5.6(2)° and 18.3(5)° for **1** and 7.8(2)° and 18.9(6)° for **2**.

The charge balance of the molecular formulae for both complexes requires that the three ligands are protonated. Unfortunately it was not possible to locate the proton positions from the last difference Fourier maps and then those protons were inserted in geometric positions bonded to the pyridine nitrogen atoms, which is in agreement with spectroscopic data. In the best of our knowledge only two X-ray single crystal structures with the $HnicO^-$ molecule were determined, the square planar complexes $[MCl(HnicO)(PPh_3)_2]$ with M equal to Pd(II) or Pt(II) [15]. In both cases the $HnicO^-$ ligand displays a monodentate coordination behaviour with the nitrogen donor atom bonded to the metal centre and consequently the proton required by the charge balance was to be found bonded to the carboxylic oxygen atom rather than to the nitrogen donor.

As described above in the crystal structure, the $HnicO^-$ bridging units act as tridentate ligands being the structural motifs that organize the 1D polymeric chains and disperse the lanthanide centres at long distances of 6.510(10) and 6.575(9) Å for **1** and **2**, respectively. These chains display a crystallographically imposed centrosymmetric structure. A comparable geometric arrangement was found in the related complex $[Eu(H_2O)(picOH)_2(\mu\text{-}HpicO)]\cdot 3H_2O$ [6], in which the $[Eu(H_2O)(picOH)_2]^+$ structural units are also covalently aggregated thorough $HpicO^-$ bridging ligands by three oxygen atoms in 1D polymeric chains. The phenolic group of the $HnicO^-$ ligand is adjacent to the nitrogen of the pyridine ring rather than the carboxylate in the $HpicO^-$ and in the $[Eu(H_2O)(picOH)_2]^+$ structural units the $picOH^-$ ligands exhibit *N*,*O*-chelation mode.

In both complexes **1** and **2** the intermolecular distances found, involving the oxygen atoms from the water molecules and the oxygen and nitrogen atoms from $HnicO^-$ ligands, suggest that in the crystal structure the polymeric chains are assembled into a 3D network via an extensive and complex system of hydrogen bonding interactions involving these atoms as donor or acceptors. However the crystal packing of these complexes is basically governed by self assembling of the 1D polymeric chains. These chains are linked by hydrogen bonds between the N–H hydrogen of a $HnicO^-$ ligand and an oxygen atom from a carboxylate group N(31)–H(31)···O(321)[$2-x, 2-y, 2-z$] with H(31)···O(321) distances of 2.07 Å in **1** and 2.07 Å in **2** (the angle N(31)–H(31)···O(321) is 153° in **1** and 156° in **2**) in a ladder type disposition in such way that the pyridine rings of adjacent chains adopt an almost parallel glide (displaced) arrangement with an intermolecular distance between them of ca. 3.20 Å in **1** and 3.30 Å in **2**, indicating that the crystal structure can also be stabilized by face-to-face π stacking interactions (see Fig. 2).

2.3. Vibrational and MAS NMR spectra

Infrared and Raman spectroscopic data for 2-hydroxynicotinic acid (H_2nicO) and its lanthanide complexes are shown in Table 2. Tentative assignments are based on those found in the literature for H_2nicO d-transition metal complexes [15]. Only the bands more sensitive to metal coordination [16,17] are reported.

The infrared spectrum of H_2nicO shows a weak band at 3229 cm^{-1} assigned to the ν(N–H) stretch from the protonated pyridinic nitrogen [15,30–33]; the in-plane δ(NH) bend at 1606 cm^{-1} and the out-of-plane γ(NH) bend at 539 cm^{-1} are also shown in the infrared and Raman spectra of H_2nicO. These features suggest that the solid H_2nicO is possibly in the ketone rather than the enol form (Scheme 1); accordingly, a strong band at 1741 cm^{-1}, assigned to the ketone ν(C=O) stretch, is also shown in the infrared and Raman spectra. A similar behaviour was reported for 2-mercaptonicotinic acid that in the solid state exists in the thione rather than the thiol form [34].

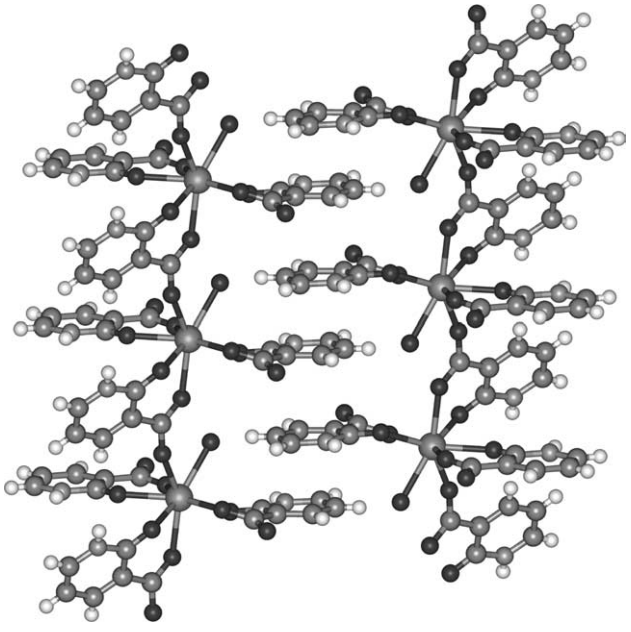

Fig. 2. Crystal packing diagram of **1** showing the π–π stacking between the polymeric chains.

The infrared and Raman spectra are very similar for all the $HnicO^-$ lanthanide complexes, suggesting that these compounds are isostructural, as shown by the crystal structures for the europium and terbium complexes. The spectroscopic data show that *O*,*O*-chelation of $HnicO^-$ is present in all the complexes. The band assigned to the ketone ν(C=O) stretch in the ligand (1741 cm^{-1}) is not seen in the infrared and Raman spectra of the lanthanide complexes, in agreement with the coordination of the respective oxygen atom to the lanthanide(III) ions. The asymmetric mode $\nu_{as}(CO_2)$ of the carboxylate group shows 10 cm^{-1} shifts to higher wavenumber on coordination when compared to the free ligand (at 1629 cm^{-1}), showing that the carboxylate oxygen is also bound to the lanthanide. In the infrared and Raman spectra, the symmetric mode $\nu_s(CO_2)$ shows higher shifts (around 30 cm^{-1}) to lower wavenumber on coordination (Table 2). The in-plane δ(NH) bend and the out-of-plane γ(NH) bend (at 1606 and 539 cm^{-1} in the free ligand, respectively) are also shown in the infrared and Raman spectra of the lanthanide complexes (at about 1600 and 538 cm^{-1}, respectively), suggesting that the pyridine nitrogen is also protonated in the complexes; the ν(N–H) stretch is obscured in the complexes by the very strong and broad ν(O–H) band (around 3411 cm^{-1}).

The ^{13}C cross-polarization (CP) magic-angle spinning (MAS) NMR spectrum of the europium complex **2** recorded with a spinning rate of 7 kHz (Fig. 3) displays a broad signal in the range 100–140 ppm, with a relatively large number of very intense spinning sidebands. This is clearly due to the interaction of ^{13}C nuclei with paramagnetic Eu^{3+} ions, thus showing that the ligands are in close spatial proximity of the lanthanide metal. A much better quality spectrum may be obtained by spinning at 15 kHz. However, because fast MAS removes the ^1H–^{13}C dipolar interaction, the cross-polarization efficiency is very low. Thus, the 15 kHz ^{13}C NMR spectrum was recorded without CP and using high-power ^1H decoupling. The optimized relaxation delay was only 5 s, indicating a short spin-lattice relaxation time (T_1) due to interaction with the Eu^{3+} ions. In addition, because (when not using CP) the 4 mm double-bearing MAS probe used as a broad background in the range ca. 100–180 ppm and echo pulse sequence was used to remove it.

Table 2
Spectroscopic data for 2-hydroxynicotinic acid and its lanthanide complexes

Compound	Vibrational spectra[a] (cm^{-1})		
	$\nu_{as}(CO_2)$	ν(CC), ν(CN)	$\nu_s(CO_2)$
2-Hydroxynicotinic acid	1629vs *1628(1)*	1550vs *1554(10)*	1413vs *1422(1)*
$[Eu(HnicO)_2(\mu\text{-}HnicO)(H_2O)]\cdot 1.25H_2O$	1639vs	1550vs *1553(10)*	1387s *1384(2)*
$[Gd(HnicO)_2(\mu\text{-}HnicO)(H_2O)]\cdot 6H_2O$	1639vs	1550vs *1553(10)*	1386w *1371(4)*
$[Tb(HnicO)_2(\mu\text{-}HnicO)(H_2O)]\cdot 1.75H_2O$	1639vs	1552vs *1553(10)*	1388s *1384(2)*
$[Er(HnicO)_2(\mu\text{-}HnicO)(H_2O)]\cdot 4H_2O$	1639vs	1552vs *1554(10)*	1383s *1371(3)*
$[Tm(HnicO)_2(\mu\text{-}HnicO)(H_2O)]\cdot 2H_2O$	1639vs	1549s *1552(10)*	1381s *1376(3)*

[a] Infrared and Raman (in italics) data; vs, very strong; s, strong; w, weak.

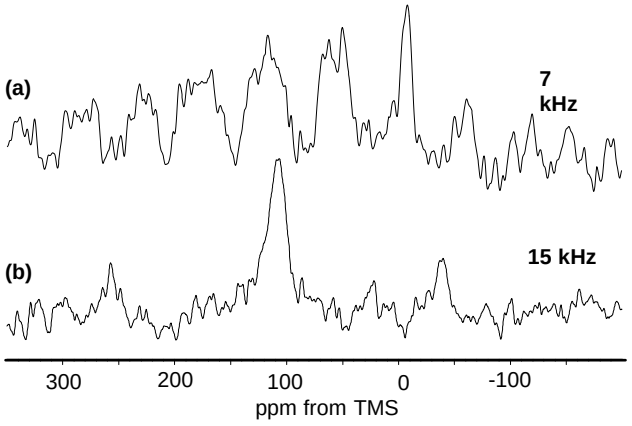

Fig. 3. ^{13}C MAS NMR spectra of $[Eu(HnicO)_2(\mu\text{-}HnicO)(H_2O)]\cdot 1.25H_2O$ (**2**) recorded with (a) cross-polarization (^1H 90° pulse 3.5 μs, contact time 2 ms) and 7 kHz spinning rate; (b) 90°–τ–180°–τ-acquisition echo pulse sequence ($\tau = 398$ μs, ^{13}C 90° pulse 1.5 μs,) high power ^1H decoupling during acquisition, and 15 kHz spinning rate.

The recorded spectrum (Fig. 3) displays a peak at ca. 108 ppm.

2.4. Photoluminescence spectra

Fig. 4(a) and (b) reproduce the room-temperature, RT, photoluminescence, PL, spectra of the Eu(III) and Tb(III) powder complexes excited at 395 and 344 nm, respectively. These excitation wavelengths correspond to the maximum intensity of the respective excitation spectra, as we will present next. The spectra are composed of a series of straight lines assigned to transitions between the first excited state ($^5D_0$ and $^5D_4$, for Eu^{3+} and Tb^{3+}, respectively) and the ground multiplet ($^7F_{0-4}$ and $^7F_{6-3}$, for Eu^{3+} and Tb^{3+}, respectively). For both complexes no emission intensity from the ligands could be detected. Comparing this latter result with the RT PL

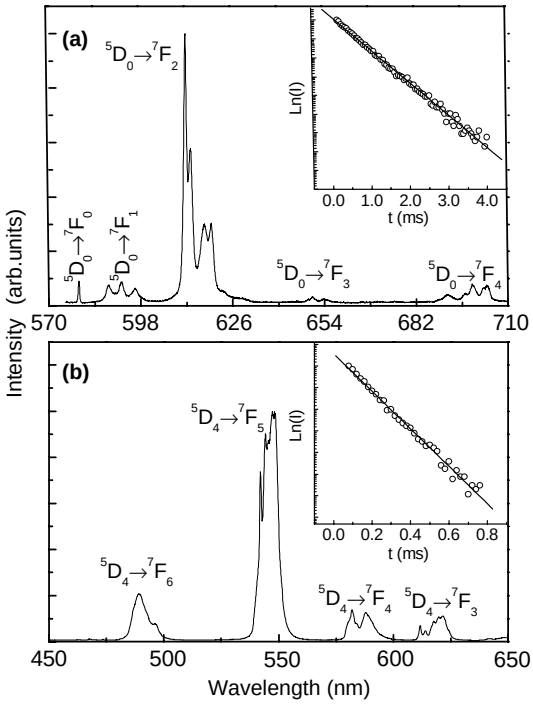

Fig. 4. RT PL spectra of the (a) $[Eu(HnicO)_2(\mu\text{-}HnicO)(H_2O)]\cdot 1.25H_2O$ and (b) $[Tb(HnicO)_2(\mu\text{-}HnicO)(H_2O)]\cdot 1.75H_2O$. The insets in (a) and (b) show the respective RT decay curves monitored around 611.5 and 544.0 nm, respectively, under 395 and 344 nm excitation wavelength. The solid line represents the data best fits, assuming a single exponential function ($r > 0.99$).

features of a series of recently proposed lanthanide based-complexes of 3-hydroxypicolinic acid, HpicOH [6], we can readily state that the ligand-to-metal energy transfer processes associated with the Tb^{3+}-based complexes with H_2nicO ligands are more efficient than those ascribed to the HpicOH ones. This conclusion is based on the fact that in the case of $[Tb(picOH)_2(\mu\text{-}HpicO)$

$(H_2O)] \cdot 3H_2O$, a large broad band associated with emission from the ligand levels was observed in the respective PL spectrum [6]. The $[Er(HnicO)_2(\mu\text{-}HnicO)(H_2O)] \cdot 4H_2O$ complex displays a weak RT emission around 1.54 μm assigned to the intra-$4f^{11}$ transition between the $^4I_{13/2}$ and $^4I_{15/2}$ levels of the Er^{3+} ground multiplet (not shown).

Fig. 5 illustrates the RT excitation spectra, PLE, for the Eu(III) and Tb(III) complexes monitored around the more intense cation emission line. The spectra are composed of a large broad band centred around 350 and 344 nm, for the Eu(III) and Tb(III) complexes, respectively, which is overlapped by a series of straight lines corresponding to the Eu^{3+} intra-$4f^6$ transitions, $^7F_0 \rightarrow {}^5G_J$, $^5L_6$, $^5D_{3-1}$, and Tb^{3+} intra-$4f^8$, $^7F_6 \rightarrow {}^5G_6$, $^5D_4$. The large broad band is also observed in the PLE spectrum of the H_2nicO ligand, peaking around 360 nm (see inset of Fig. 5). The incorporation of the lanthanide ions produce a blue-shift of the ligands energy levels (≈794 cm^{-1}, Eu^{3+}, ≈1291 cm^{-1}, Tb^{3+}), indicating an effective interaction between the two lanthanide ions and the H_2nicO ligand. Moreover, the intensity of the metal-centred transitions is strong, relatively to that of the broad ligand band, which actually implies that direct metal excitation is comparable with the sensitized process, as the extinction coefficients of the metal emission are much lower than that of the ligands. On the contrary, the ligand-to-metal energy transfer seems to be more efficient in the $[Eu(picOH)_2(\mu\text{-}HpicO)(H_2O)] \cdot 3H_2O$ complex, as the integrated intensity of the broad band is much larger than that of the f–f lines (the sensitized process is clearly much more important than the direct metal excitation), inset of Fig. 3(b) of [6].

The diffuse reflectance spectra of the H_2nicO ligand and the Eu(III) and Tb(III) complexes are shown in Fig. 6. The spectra are very similar, consisting of a large broad absorption bands in the UV region at approximately 220–380 nm. The maximum of this band shifts towards lower wavelengths in the complexes, relative to the ligand, in accordance with the PLE spectra.

The RT lifetime of the Eu^{3+} and Tb^{3+} first excited state was monitored around the more intense transition of the cation (see insets of Fig. 4(a) and (b), respectively). The decay curve is well described by a single exponential, indicating a single and homogeneous local coordination site for the lanthanide ions. The fit of the experimental data revealed lifetimes of 0.592 ± 0.007 and 0.113 ± 0.002 ms for the Eu^{3+} and Tb^{3+} emitting state, $^5D_0$ and $^5D_4$, respectively.

Due to the particular characteristics of the Eu^{3+} energy levels, we are able to estimate the efficiency, q, of the emission arising from the $^5D_0$ level [6,35,36]. Assuming that only non-radiative and radiative processes are essentially involved in the depopulation of the $^5D_0$ state, q can be defined as $q = k_r/(k_r + k_{nr})$, where k_r and k_{nr} are the radiative and non-radiative probabilities,

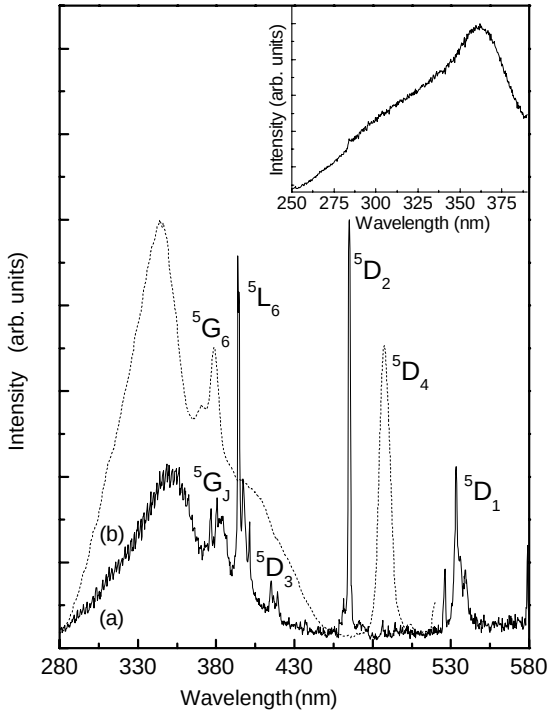

Fig. 5. RT PLE spectra of the (a) $[Eu(HnicO)_2(\mu\text{-}HnicO)(H_2O)] \cdot 1.25H_2O$ and (b) $[Tb(HnicO)_2(\mu\text{-}HnicO)(H_2O)] \cdot 1.75H_2O$ monitored around 611.5 and 544.0 nm, respectively. The inset shows the RT PLE spectrum of the H_2nicO ligand monitored around 420 nm.

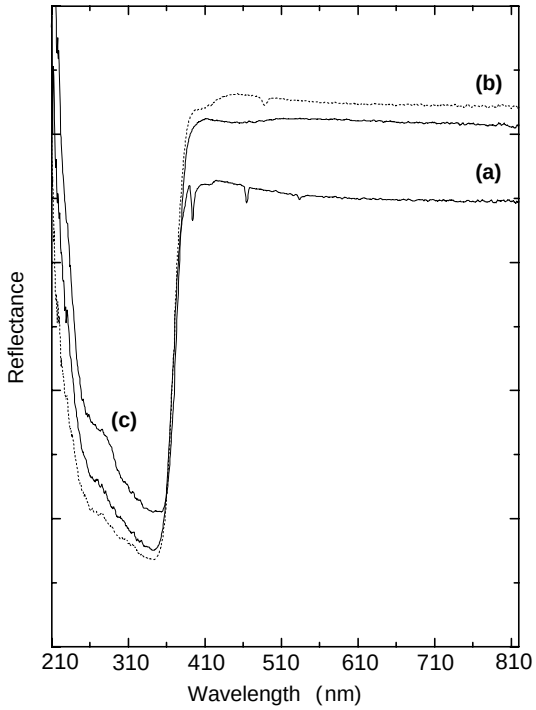

Fig. 6. RT diffuse reflectance spectra of (a) $[Eu(HnicO)_2(\mu\text{-}HnicO)(H_2O)] \cdot 1.25H_2O$, (b) $[Tb(HnicO)_2(\mu\text{-}HnicO)(H_2O)] \cdot 1.75H_2O$ and (c) H_2nicO ligand.

respectively. The emission intensity, I, taken as the integrated intensity of the $^5D_0 \rightarrow {}^7F_{0-4}$ emission lines, can be expressed by

$$I_{i\rightarrow j} = \hbar w_{i\rightarrow j} A_{i\rightarrow j} N_i, \quad (1)$$

where i and j represent the initial ($^5D_0$) and final levels ($^7F_{0-4}$), respectively, $\hbar w_{i\rightarrow j}$ is the transition energy, $A_{i\rightarrow j}$ corresponds to Einstein's coefficient of spontaneous emission and N_i is the population of the $^5D_0$ emitting level [6,37,38]. The radiative contribution, k_r, may be calculated from the relative intensities of the $^5D_0 \rightarrow {}^7F_{0-4}$. Since the $^5D_0 \rightarrow {}^7F_1$ transition can be considered as a reference, due to its dipolar magnetic nature, k_r, can be calculated as [6,35,36]

$$k_r = \frac{A_{0-1}E_{0-1}}{S_{0-1}} \sum_{J=0}^{4} \frac{S_{0-J}}{E_{0-J}}, \quad (2)$$

where A_{0-1} is Einstein's coefficient of spontaneous emission between the $^5D_0$ and the $^7F_1$ levels, which is usually referenced as equal to 50 s^{-1} [6,19,20], E_{0-J} and S_{0-J} are the energy and the integrated intensity of the $^5D_0 \rightarrow {}^7F_J$ transition, respectively. The parameter k_{nr} can be calculated from the $^5D_0$ experimental decay time, τ, considering that $k_{exp} = \tau^{-1} = k_{rad} + k_{nrad}$. We obtained a q value of $\approx 29.2\%$ for the Eu^{3+} emission in the $HnicO^-$ complex, with corresponding k_r and k_{nr} values of $\approx$0.494 and $\approx$1.195 ms^{-1}, respectively. These values are different from those calculated for the Eu^{3+} complex involving the HpicOH ligand, while the quantum efficiency value and the radiative transition probability are higher than the values observed for the Eu^{3+} complex involving the HpicOH ligand ($q \approx 13.5\%$ and $k_r \approx 0.281$ ms^{-1}) the non-radiative transition probability is smaller ($k_{nr} \approx 1.785$ ms^{-1}) [6].

The luminescence quenching of rare earth ions is usually associated with the presence of water molecules coordinated to the ion. Assuming the presence of OH oscillators as responsible for the non-radiative component of the experimental transition probability, we can infer the number of coordinated water molecules, n_w, though the empirical formula suggested by Horrocks and co-workers [39], $n_w = 1.05 \times (k_{exp} - k_r)$. We found that the number of water molecules, which belong to the Eu^{3+} first coordination shell is 1.3 ± 0.5. This result is consistent with the single crystal X-ray diffraction results discussed in the previous section.

In the next paragraphs we will interpret the observed differences between the HpicOH ligand and the H_2nicO ligand, namely, the more efficient ligand-to-metal energy transfer mechanisms performed by the latter ligand for the Tb^{3+} ions and the greater q value found for the $[Eu(HnicO)_2(\mu\text{-}HnicO)(H_2O)] \cdot 1.25H_2O$ complex, in spite of the less efficient ligand-to-metal energy transfer, relatively to the Eu^{3+} complex with HpicOH ligand.

In the PLE spectra monitored around the Eu^{3+} and Tb^{3+} emission lines the band ascribed to the HpicOH ligands is centred at ca. 26660 cm^{-1} (375 nm), which corresponds to the same energy found in the PLE spectrum of the non-coordinated HpicOH ligand [6]. However, in the case of the H_2nicO complex there is a blue-shift of the energy of the band that corresponds to the excitation of the ligands levels in the spectra monitored around the ions emission lines, when compared with the energy found in the PLE spectra of the non-coordinated ligand, being around 28 571 cm^{-1} (350 nm) and 29 070 cm^{-1} (344 nm) for the Eu^{3+} and Tb^{3+}-based complexes, respectively. These results suggest a more effective interaction between the lanthanide ions and the ligands in the case of the H_2nicO-based complexes. The energy of the ligands, HpicOH and H_2nicO, levels in the presence of the Eu^{3+} and Tb^{3+} ions can be estimated by analysing the luminescence of the respective Gd^{3+}-based complexes. This experimental procedure is based on the fact that the Gd^{3+} excited levels have energies much higher than those typical of ligand singlet and triplet states, disabling, thus, any ligand-to-metal energy transfer process. In this way, the luminescence spectra will be composed by transitions arising from the singlet and triplet ligands levels. Fig. 7 shows the emission spectra arising from the Gd^{3+}-based complexes involving H_2nicO and HpicOH ligands, excited at 340 and 355 nm, respectively. These spectra were measured at low-temperature, 10 K, in order to achieve greater intensity and resolution in the energy levels assignment. The emission spectrum of $[Gd(HnicO)_2(\mu\text{-}HnicO)(H_2O)] \cdot 6H_2O$ displays two peaks, centred around 475 nm (21 053 cm^{-1}), 507 nm (19 724 cm^{-1}) ascribed to a resolvable vibrational fine structure originating from a single triplet state or to the lowest three triplet states of each one of the three H_2nicO ligands. The fact that the two peaks separation in energy is ca. 1329 cm^{-1}, which approximately corresponds to a vibrational progression typical of the $n\pi*$ emission of aromatic molecules [40,41], supports the former suggestion. In the emission spectrum of $[Gd(picOH)_2(\mu\text{-}HpicO)(H_2O)] \cdot 5H_2O$, red-shifted regarding that of the Gd H_2nicO complex, only one peak is unequivocally distinguished, centred at ca. 519 nm (19 268 cm^{-1}). However, the shape of the emission curve is clearly associated with more than one Gaussian curve in accordance with a vibrational fine structure.

Fig. 8 shows the excitation PLE spectra for both Gd^{3+}-based complexes monitored around the more intense emission peak. The spectra reveal a large broad band centred around 340 and 355 nm for the complexes with H_2nicO and HpicOH, respectively. The RT diffuse reflectance spectrum (see inset of Fig. 8) of each complex also indicates that the maximum absorption occurs around the same excitation wavelengths extracted from the low-temperature PLE spectra.

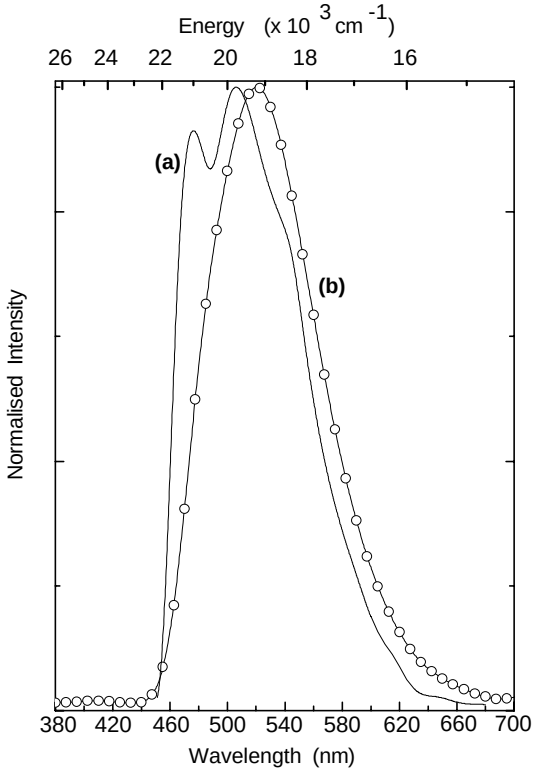

Fig. 7. Low-temperature (10 K) PL spectra of the (a) $[Gd(HnicO)_2(\mu\text{-}HnicO)(H_2O)]\cdot 6H_2O$ and (b) $[Gd(picOH)_2(\mu\text{-}HpicO)(H_2O)]\cdot 5H_2O$.

The energetic position of the singlet (S) and triplet (T) states relative to each ligand were extracted from the previous analyses of the excitation and emission spectra measured at 10 K for Gd^{3+}-based complexes. The energy of the triplet state was estimated from the shortest-wavelength peak of the PL emission spectra, whereas the energy of the singlet was extracted from the absorption edges in the diffuse reflectance spectra (assuming that it corresponds 0 $(S_0) \rightarrow 0$ (S_1) transition). This energy can be also determined from the PLE spectra of the Gd^{3+}-based complexes. Fig. 9 shows the energetic position of the singlet and triplet states relative to the H_2nicO and HpicOH ligands and the Eu^{3+} and Tb^{3+} intra-4f levels.

The singlet and triplet energy of HpicOH are red-shifted with respect to the H_2nicO levels. Focussing first on the Tb^{3+}-based complexes, there is a higher resonance between the HpicOH singlet and the $^5L_{10}$ and $^5D_3$ levels. Although it might contribute to a greater energy transfer to the lanthanide ion, it also increases the probability of back transfer from the lanthanide levels. Moreover, the HpicOH energy of the triplet state lies below the Tb^{3+} emitting state ($^5D_4$), so that the energy transfer mechanisms from the ligands to the Tb^{3+} ions are not favoured and radiative emission from the ligands triplet levels occurs. In the complexes with H_2nicO, the ligands triplet state is almost resonant with the $^5D_4$ level,

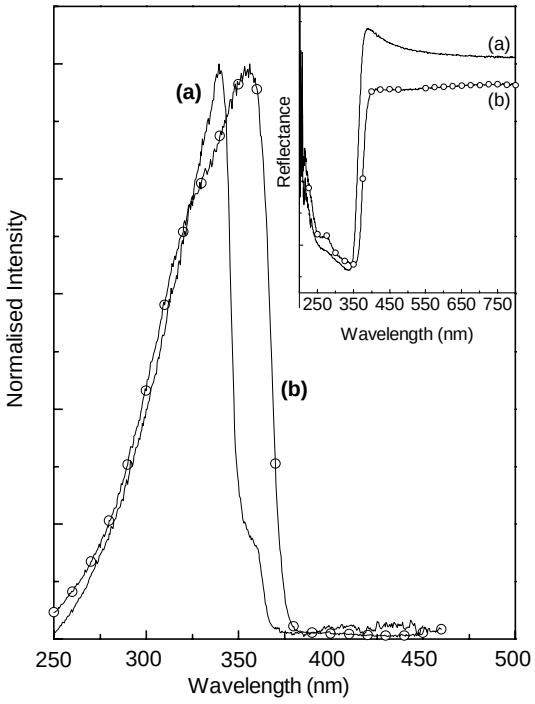

Fig. 8. Low-temperature (10 K) PLE spectra of the (a) $[Gd(HnicO)_2(\mu\text{-}HnicO)(H_2O)]\cdot 6H_2O$ and (b) $[Gd(picOH)_2(\mu\text{-}HpicO)(H_2O)]\cdot 5H_2O$ monitored around 479 and 520 nm, respectively. The inset shows the RT diffuse reflectance spectra of the previous complexes.

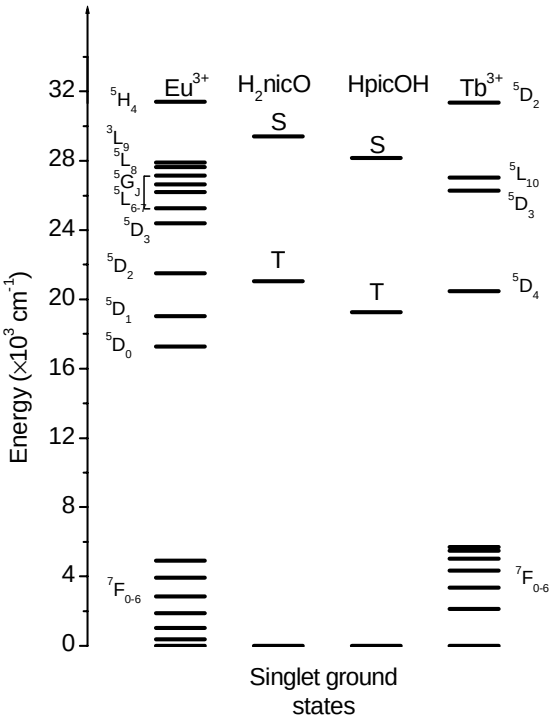

Fig. 9. Schematic illustration of the energy diagram for Eu^{3+}, Tb^{3+} and ligand singlet and triplet levels in $[Ln(HnicO)_2(\mu\text{-}HnicO)(H_2O)]\cdot nH_2O$ and $[Ln(H_2O)(picOH)_2(\mu\text{-}HpicO)]\cdot 3H_2O$ (Ln = Eu and Tb).

so that efficient energy transfer occurs from the triplet to that level, disabling the ligands emission.

In the Eu^{3+}-based complexes both ligands provide energy transfer to the lanthanide emitting level. In both cases the greater overlap occurs between the triplet state and the $^5D_1$ level. Malta et al. [42] reported that the most efficiency energy transfer occurs between the triplet states and the $^5D_1$ level, through the so-called exchanging mechanism. As the triplet states are more resonance with the $^5D_1$ level in the complex with HpicOH, relatively to the complex with H_2nicO (Fig. 9), the ligand-to-metal energy transfer should be more efficient in the former complex, which is exactly the conclusion inferred from the excitation spectra discussed previously. In any case, this resonance induces the observed absence of the ligands contribution in the emission spectra of both complexes. However, a greater q value was obtained for the complexes with H_2nicO (29.2%) than that calculated for $[Eu(picOH)_2(\mu\text{-}HpicO)(H_2O)]\cdot 3H_2O$ (13.5%) [6]. This may also be interpreted through the analysis of the relative position between the triplet states and the $^5D_0$ emitting level. The greater overlap between this level and the triplet level occurs for the complex with HpicOH, increasing the probability of phonon-assisted energy back-transfer from the $^5D_0$ level to the triplet state. This will disregard the population of the $^5D_0$ level and contribute to decrease its quantum efficiency. Moreover, water molecules belonging to the first coordination shell contribute for that phonon-assisted back-transfer mechanism. Despite the same number of water molecules in the first coordination shell for both complexes (one), in $[Eu(HnicO)_2(\mu\text{-}HnicO)(H_2O)]\cdot 1.25H_2O$ the water molecule is more far away from the central ion than in $[Eu(picOH)_2(\mu\text{-}HpicO)(H_2O)]\cdot 3H_2O$ (2.514 and 2.389 Å, respectively). This is an additional argument supporting the relative minor importance of the phonon-assisted back-transfer mechanism in the Eu^{3+}-HnicO complex.

3. Experimental

All chemicals were supplied by Aldrich and used as received.

3.1. Preparation of $[Ln(HnicO)_2(\mu\text{-}HnicO)(H_2O)]\cdot nH_2O$ (Ln = Eu, Gd, Tb, Er, Tm)

The lanthanide complexes were prepared by adding aqueous solutions (5 ml) of the respective lanthanide salt (0.5 mmol), $LnX_3\cdot nH_2O$ (Ln = Eu, Gd, Er, Tm and X = Cl; Ln = Tb and X = NO_3), to an aqueous solution (15 ml, pH 6.0) of 2-hydroxynicotinic acid (2 mmol) and KOH (2 mmol). After stirring the mixture over one hour, the solid formed was collected by filtering and then washed thoroughly with distilled water. Crystals of **1** and **2** were obtained by recrystallization from aqueous solutions of the respective powders, after slow evaporation over two months. *Anal.* Calc. for $[Eu(HnicO)_2(\mu\text{-}HnicO)(H_2O)]\cdot 1.25H_2O$: C 35.63; N 6.92; H 2.74. Found: C 32.81; N 6.69; H 3.54%. Calc. for $[Gd(HnicO)_2(\mu\text{-}HnicO)(H_2O)]\cdot 6H_2O$: C 30.99; N 6.03; H 3.73. Found: C 30.62; N 5.90; H 3.14%. Calc. for $[Tb(HnicO)_2(\mu\text{-}HnicO)(H_2O)]\cdot 1.75H_2O$: C 34.71; N 6.75; H 2.83. Found: C 33.12; N 6.83; H 2.87%. Calc. for $[Er(HnicO)_2(\mu\text{-}HnicO)(H_2O)]\cdot 4H_2O$: C 32.19; N 6.26; H 3.28. Found C 32.15; N 6.43; H 3.25%. Calc. for $[Tm(HnicO)_2(\mu\text{-}HnicO)(H_2O)]\cdot 2H_2O$: C 33.91; N 6.59; H 2.83. Found C 33.75; N 7.84; H 2.27%.

3.2. Preparation of $[Gd(picOH)_2(\mu\text{-}HpicO)(H_2O)]\cdot 5H_2O$

The gadolinium 3-hydroxypicolinate complex $[Gd(picOH)_2(\mu\text{-}HpicO)(H_2O)]\cdot 5H_2O$ was synthesized using our earlier reported method [6] for other lanthanide complexes. $Gd(OH)_3$ was prepared by adding aqueous solutions (5 ml) of KOH (3 mmol) to an equal volume of aqueous solutions containing the gadolinium chloride salt (1 mmol). The solid formed was stirred over 90 min, filtered and washed thoroughly with distilled water. The 3-hydroxypicolinate gadolinium complex was prepared by adding 1 mmol of $Gd(OH)_3$ to an aqueous solution (25 ml) containing 3-hydroxypicolinic acid (4 mmol). This mixture was stirred during 1 h, then heated for 30 min at 80 °C, and further stirred over eight hours at room temperature. The solid obtained was filtered, washed thoroughly with distilled water and dried over silica gel. *Anal.* Calc. for $[Gd(picOH)_2(\mu\text{-}HpicO)(H_2O)]\cdot 5H_2O$: C 31.81; N 6.18; H 3.56. Found C 31.29; N 6.01; H 2.41%. Selected bands from infrared (solid, KBr pellet, ν/cm^{-1})/Raman (solid, ν/cm^{-1}, in italics) spectra and tentative assignments [6]: 3424 [ν(O–H)]; 1625/*1626* [$\nu_{as}(CO_2)$]; 1592/*1591* [ν(C–N)]; 1343/*1322* [$\nu_s(CO_2)$]; 1261/*1261* [$\nu(C\text{–}O)_h$].

3.3. Crystallography

The pertinent crystallographic data for complexes **1** and **2** are summarized in Table 3.

X-ray data were collected at room temperature on a MAR research plate system using graphite monocromatized Mo Kα radiation ($\lambda = 0.71073$ Å) at Reading University. The crystals were positioned at 70 mm from the image plate. 95 frames were taken at 2° intervals using a counting time of 5 min. Data analysis was performed with XDS program [43]. Intensities were corrected empirically for absorption effects, using a DIFABS version modified for image plate geometry [44].

The structure was solved by direct methods and by subsequent difference Fourier syntheses and refined by

Table 3
Crystal data and pertinent refinement details for complexes **1** and **2**

Compound	**1**	**2**
Empirical formula	$C_{18}H_{17.50}N_3O_{11.75}Tb$	$C_{18}H_{16.50}N_3O_{11.25}Eu$
Formula weight	622.77	606.80
Crystal system	triclinic	triclinic
Space group	$P\bar{1}$	$P\bar{1}$
Unit cell dimensions		
a (Å)	6.510(9)	6.575(9)
b (Å)	13.076(15)	12.897(15)
c (Å)	14.554(16)	14.645(17)
α (°)	82.22(1)	82.89(1)
β (°)	80.86(1)	80.79(1)
γ (°)	82.70(1)	83.77(1)
Volume (Å^3)	1205	1211(3)
Z	2	2
Calculated density (Mg m^{-3})	1.729	1.696
Absorption coefficient (mm^{-1})	2.999	2.652
Reflections collected	5994	7318
Unique reflections [R_{int}]	4071 [0.0589]	4197 [0.0732]
Data/restraints/parameters	4071/0/316	4197/0/307
Final R indices $[I > 2\sigma(I)]R_1$ and wR_2	0.0674, 0.1858	0.0577, 0.1516
R indices (all data) R_1 and wR_2	0.0710, 0.1883	0.0641, 0.1553
Largest difference peak and hole (eÅ^{-3})	−1.588 to 2.090	−1.013 to 1.503

full matrix least squares on F^2 using the SHELX-97 system programs [45].

The hydrogen atoms on the parent carbon atoms and pyridine nitrogen atoms were included in calculated positions and given thermal parameters equivalent 1.2 times those of the atom to which were attached. The hydrogen atoms of the water molecules were not revealed by the successive Fourier maps and their positions were not introduced in the refinement. The last difference Fourier maps calculated showed residual electronic densities in the range −1.59 to 2.10 eÅ^{-3} for **1** and −1.01 to 1.50 for **2**, with the highest positive peak within the corresponding metal coordination sphere.

3.4. Instrumentation

All the lanthanide complexes were characterized by infrared, Raman, NMR, diffuse reflectance and photoluminescence spectroscopies, and elemental analysis. Infrared spectra were measured as KBr disks using a Mattson 7000 FT instrument. Raman spectra were recorded using a Brüker RFS100/S FT-Raman spectrometer (Nd:YAG laser, 1064 nm excitation). Diffuse reflectance spectra were measured on a JASCO V-560 instrument. ^{13}C NMR spectra have been recorded on a Bruker Avance 400 at 100.6 MHz, details are given in the text and in the caption of Fig. 3. Microanalyses (C, H and N) were measured in the Department of Chemistry, University of Aveiro.

The emission, PL, and excitation, PLE, spectra (10–300 K) of the Eu^{3+} and Tb^{3+} powder complexes were recorded on a Jobin Yvon-Spex spectrometer (HR 460) coupled to a R928 Hamamatsu photomultiplier. A 150 W Xe arc lamp coupled to an excitation monochromator Jobin Yvon-Spex (TRIAX 180) was used as excitation source. The RT infrared emission of the Er(III) compound was detected on a Bruker IFS 66v Fourier transform infrared (FTIR) coupled to a Ge North-West-Coast EO-817 photodiode cooled to 77 K. The 514.5 nm line of an Ar ion-laser was used as excitation source. The RT lifetime measurements were carried out using a pulsed Xe arc lamp (5 mJ/pulse, 3 μs bandwidth) coupled to a Kratos GM-252 monochromator and a Spex 1934 C phosphorimeter.

Acknowledgements

P. Soares-Santos thanks the University of Aveiro for a Ph.D. research grant. R.A. Sá Ferreira thanks the Fundação para a Ciência e Tecnologia (FCT) for a grant SFRH/BPD/11480/2002. The authors thank the financial support from FCT (Grant contract: POCTI/35378/QUI/2000 and POCTI/33653/CTM/2000) supported by FEDER.

References

[1] G.F. Sá, O.L. Malta, C.M. Donegá, A.M. Simas, R.L. Longo, P.A. Santa-Cruz, E.F. Silva Jr., Coord. Chem. Rev. 196 (2000) 165.
[2] G. Vicentini, L.B. Zinner, J. Zukerman-Schpector, K. Zinner, Coord. Chem. Rev. 196 (2000) 353.
[3] J.M. Lehn, Angew. Chem., Int. Ed. Engl. 29 (1990) 1304.
[4] S.W. Magennis, S. Parsons, Z. Pikramenou, Chem. Eur. J. 8 (2002) 5761.

[5] S.W. Magennis, S. Parsons, A. Corval, J.D. Woollins, Z. Pikramenou, Chem. Commun. 8 (1999) 61.
[6] P.C.R. Soares-Santos, H.I.S. Nogueira, V. Félix, M.G.B. Drew, R.A. Sá Ferreira, L.D. Carlos, T. Trindade, Chem. Mater. 15 (2003) 100.
[7] P.C.R. Soares-Santos, H.I.S. Nogueira, V. Félix, M.G.B. Drew, R.A. Sá Ferreira, L.D. Carlos, T. Trindade, Inorg. Chem. Commun. 6 (2003) 1234.
[8] P.C.R. Soares-Santos, H.I.S. Nogueira, F.A. Almeida Paz, R.A. Sá Ferreira, L.D. Carlos, J. Klinowski, T. Trindade, Eur. J. Inorg. Chem. (2003) 3609.
[9] A.I. Krasnova, M.P. Aguillar-Cabalhos, A. Gómez-Hens, Anal. Chim. Acta 441 (2001) 249.
[10] B. Yan, H. Zhang, S. Wang, J. Ni, J. Photochem. Photobiol. A 112 (1998) 231.
[11] Y.J. Park, B.H. Lee, W.H. Kim, Y. Do, J. Colloid Interface Sci. 209 (1999) 268.
[12] J.B. Lamture, Z.H. Zhou, A.S. Kumar, T.G. Wensel, Inorg. Chem. 34 (1995) 864.
[13] J.G. Bünzli, L.J. Charbonnière, R.F. Ziessel, J. Chem. Soc., Dalton Trans. (2000) 1917.
[14] D.M.L. Goodgame, S.P.W. Hill, A.M. Smith, D.J. Williams, J. Chem. Soc., Dalton Trans. (1994) 859.
[15] S.M.O. Quintal, H.I.S. Nogueira, V. Félix, M.G.B. Drew, Polyhedron 21 (2002) 2783.
[16] C.F. Edwards, W.P. Griffith, A.J.P. White, D.J. Williams, J. Chem. Soc., Dalton Trans. (1993) 3813.
[17] W.P. Griffith, H.I.S. Nogueira, B.C. Parkin, R.N. Sheppard, A.J.P. White, D.J. Williams, J. Chem. Soc., Dalton Trans. (1995) 1775.
[18] M.S. Saleh, K.A. Idriss, M.S. Abu-Bakr, E. Hashem, Analyst 117 (1992) 1003.
[19] A.K.W. Stephens, C. Orvig, Inorg. Chim. Acta 273 (1998) 47.
[20] E. Kiss, K. Petrohán, D. Sanna, E. Garribba, G. Micera, T. Kiss, Polyhedron 19 (2000) 55.
[21] R. Bertani, G.G. Bombi, A. Tapparo, Rapid Commun. Mass Spectrosc. 13 (1999) 1878.
[22] V.B. Di Marco, A. Tapparo, G.G. Bombi, Ann. Chim. 89 (1999) 535.
[23] K.A. Idriss, M.S. Saleh, E.Y. Hashem, Bull. Polish Acad. Sci. 43 (1995) 67.
[24] M.S. Saleh, J. Indian Chem. Soc. 70 (1993) 202.
[25] K.A. Idriss, M.S. Saleh, H. Sedaira, Monatsh. Chem. 122 (1991) 507.
[26] A.L. Spek, PLATON, a Multipurpose Crystallographic Tool, Utrecht University, Utrecht, The Netherlands, 1999.
[27] WEBLAB VIEWER, version 2.01, Molecular Simulations, Inc., San Diego, CA, 1997.
[28] A.F. Wells, Structural Inorganic Chemistry, Clarendon Press, Oxford, 1984, pp. 78 and 79.
[29] F.H. Allen, O. Kennard, Chem. Design Autom. News 8 (1993) 31.
[30] K.M. Mukherjee, T.N. Misra, J. Raman Spectrosc. 27 (1996) 595.
[31] P.A.P. Lourido, J.A.G. Vásquez, J. Romero, M.S. Louro, A. Sousa, Q. Chen, Y. Chang, J. Zubieta, J. Chem. Soc., Dalton Trans. (1996) 2047.
[32] S. Banerji, R.E. Byrne, S.E. Livingstone, Trans. Met. Chem. 7 (1982) 5.
[33] E.C. Constable, S.M. Elder, C.A. Palmer, P.R. Raithby, D.A. Tocher, Inorg. Chim. Acta 252 (1996) 281.
[34] S.M.O. Quintal, H.I.S. Nogueira, V. Félix, M.G.B. Drew, J. Chem. Soc., Dalton Trans. (2002) 4479.
[35] L.D. Carlos, Y. Messaddeq, H.F. Brito, R.A. Sá-Ferreira, V. de Zea Bermudez, S.J.L. Ribeiro, Adv. Mater. 12 (2000) 594.
[36] R.A. Sá Ferreira, L.D. Carlos, R.R. Gonçalves, S.J.L. Ribeiro, V. de Zea Bermudez, Chem. Mater. 13 (2001) 2991.
[37] O.L Malta, M.A. Couto dos Santos, L.C. Thompson, N.K. Ito, J. Lumin. 69 (1996) 77.
[38] O.L Malta, H.F. Brito, J.F.S. Menezes, F.R. Gonçalves e Silva, S. Alves Jr., F.S. Farias Jr., A.V.M. Andrade, J. Lumin. 75 (1997) 255.
[39] W.D. Horrocks Jr., W.D.R. Sudnick, Acc. Chem. Res. 14 (1981) 384.
[40] S. Jockusch, G. Dedola, G. Lem, N.J. Turro, J. Phys. Chem. 103 (1999) 9126.
[41] K. Ray, A. Shanzer, D.H. Waldeck, R. Naaman, Phys. Rev. B. 60 (1999) 13347.
[42] O.L. Malta, F.R. Gonçalves e Silva, Spectrochim. Acta, Part A 54 (1998) 1593.
[43] W. Kabsch, J. Appl. Crystallogr. 21 (1988) 916.
[44] N. Walker, D. Stuart, DIFABS, Acta Cryst., Sect. A 39 (1983) 158.
[45] G.M. Sheldrick, SHELX-97, University of Göttingen, Göttingen, 1997.